large weighting to the direction of joint movements for realizing the desired terminal conditions.

Conclusion

This Note proposes a method of path planning for space manipulators that reduces disturbances to the spacecraft attitude. The proposed method uses the EDM for planning the manipulator path in the joint space. The method sequentially determines the direction of small steps of joint movements that compromises the biobjectives of minimizing the disturbance to the spacecraft attitude and realizing the terminal end effector position. Numerical simulations have been made for a space robot with a two-link manipulator. The results of the simulations show the feasibility of the present path planning algorithm.

References

[1]Lindberg, R., Longman, R., and Zedd, M., "Kinematic and Dynamic Properties of an Elbow Manipulator Mounted on a Satellite," *Space Robotics: Dynamics and Control*, Kluwer Academic, Norwell, MA, 1993, pp. 1–25.

[2]Yamada, K., "Attitude Control of Space Robot by Arm Motion," *Journal of Guidance, Control, and Dynamics*, Vol. 17, No. 5, 1994, pp. 1050–1054.

[3]Vafa, Z., and Dubowsky, S., "On the Dynamics of Space Manipulators Using the Virtual Manipulator, with Applications to Path Planning," *Journal of the Astronautical Sciences*, Vol. 38, No. 4, 1990, pp. 441–472.

[4]Torres, M. A., and Dubowsky, S., "Minimizing Spacecraft Attitude Disturbances in Space Manipulator Systems," *Journal of Guidance, Control, and Dynamics*, Vol. 15, No. 4, 1992, pp. 1010–1017.

[5]Okubo, H., Nagano, N., Komatsu, N., and Tsumura, T., "Path Planning for Space Manipulators Using Enhanced Disturbance Map," *Proceedings of the AIAA Guidance, Navigation, and Control Conference* (Baltimore, MD), AIAA, Washington, DC, 1995, pp. 1510–1517.

Experimental Comparison of Robust $\mathcal{H}_2$ Control Techniques for Uncertain Structural Systems

Simon C. O. Grocott,* Jonathan P. How,†
and David W. Miller‡
Massachusetts Institute of Technology, Cambridge, Massachusetts 02139

I. Introduction

INCREASING performance specifications require that many future spacecraft use active structural control to meet payload pointing performance specifications. The Middeck Active Control Experiment (MACE) was developed to investigate the issues associated with developing controllers for on-orbit operations, based on ground testing. The change from 1-*g* ground tests to 0-*g* experimentation introduces uncertainty in the fidelity of ground-based models; thus, robust control techniques must be used in the design of compensators.

This Note uses experimental results from MACE ground tests to present a comparison of sensitivity-weighted linear quadratic Gaussian (SWLQG),[1] maximum entropy (ME),[2,3] and multiple model (MM)[4] control with $\mathcal{H}_2$ optimal LQG,[5] looking particularly at the robustness/performance tradeoff.

Received Dec. 29, 1995; revision received Dec. 31, 1996; accepted for publication Jan. 4, 1997. Copyright © 1997 by the American Institute of Aeronautics and Astronautics, Inc. All rights reserved.

*Research Assistant, Space Engineering Research Center. Student Member AIAA.

†Postdoctoral Associate, Space Engineering Research Center; currently Assistant Professor, Department of Aeronautics and Astronautics, Stanford University, Stanford, CA 94305. Member AIAA.

‡Principal Research Scientist, Associate Director, Space Engineering Research Center. Member AIAA.

II. $\mathcal{H}_2$ Control Techniques

Common to each of the control techniques is the system dynamics

$$\begin{aligned} \dot{x} &= Ax + B_w w + B_u u \\ z &= C_z x + D_{zw} w + D_{zu} u \\ y &= C_y x + D_{yw} w + D_{yu} u \end{aligned} \tag{1}$$

which are controlled through a dynamic compensator of the form

$$\dot{x}_c = A_c x_c + B_c y, \qquad u = C_c x_c \tag{2}$$

where w is a vector of uncorrelated white-noise disturbances with unit intensity, u is the control input vector, z is the performance vector, and y is the measurement vector.

Optimal $\mathcal{H}_2$ control (LQG)[5] minimizes the $\mathcal{H}_2$ norm (from w to z) of this system, or equivalently the cost functional

$$J = \lim_{t\to\infty} \mathbb{E}\{z^T z\} = \lim_{t\to\infty} \mathbb{E}\left\{x^T R_{xx} x + 2x^T R_{xu} u + u^T R_{uu} u\right\} \tag{3}$$

For this Note, the noise (V_{xx}, V_{xy}, V_{yy}) and performance weights (R_{xx}, R_{xu}, R_{uu}) are completely defined by the actual disturbance inputs (w) and performance variables (z) so that

$$V = \begin{bmatrix} V_{xx} & V_{xy} \\ V_{xy}^T & V_{yy} \end{bmatrix} = \begin{bmatrix} B_w \\ D_{yw} \end{bmatrix} \begin{bmatrix} B_w^T & D_{yw}^T \end{bmatrix} \geq 0, \qquad V_{yy} > 0 \tag{4}$$

and

$$R = \begin{bmatrix} R_{xx} & R_{xu} \\ R_{xu}^T & R_{uu} \end{bmatrix} = \begin{bmatrix} C_z^T \\ D_{zu}^T \end{bmatrix} [C_z \quad D_{zu}] \geq 0, \qquad R_{uu} > 0 \tag{5}$$

This definition is restrictive but results in optimal $\mathcal{H}_2$ controllers for the system in Eq. 1.

The maximum entropy[2,3] approach minimizes the cost functional [Eq. (3)] but uses a multiplicative white-noise model of parametric uncertainty in the dynamics. The maximum entropy equations of Collins et al.[3] are designed for handling uncertainty in natural frequencies of flexible structures and are used herein. The equations provide weightings (δ_i) for each mode that is considered uncertain.

The multiple model technique minimizes a weighted average of the $\mathcal{H}_2$ norms of a discrete set of models.[4] Robustness is added by selecting a set of models that have different values for uncertain parameters. In this Note, the number of models is always three: one is the nominal model, and the other two have positive and negative shifts, respectively, of each of the uncertain modes. The solution is obtained through a quasi-Newton optimization.

Finally, the SWLQG technique requires some elaboration because no complete reference is available. SWLQG is essentially an LQG problem that is suboptimal for the system in Eq. (1) but is more robust than the optimal. It provides a formal method for choosing the weights (R and V) to provide good $\mathcal{H}_2$ performance for the system with greater robustness.

Ignoring for a moment the noise input w in Eq. (1), SWLQR[1] optimizes the standard LQR cost functional with an additional quadratic term in the sensitivity states of the system

$$J = \lim_{T\to\infty} \int_0^T x^T R_{xx} x + \sum_{i=1}^{n_\alpha} \frac{\partial x^T}{\partial \alpha_i} R_{\alpha\alpha_i} \frac{\partial x}{\partial \alpha_i} + 2x^T R_{xu} u + u^T R_{uu} u \, dt \tag{6}$$

where $\partial x/\partial \alpha_i$ is the sensitivity state vector and is obtained by differentiating Eq. (1) to yield

$$\frac{\partial \dot{x}}{\partial \alpha_i} = A\frac{\partial x}{\partial \alpha_i} + \frac{\partial A}{\partial \alpha_i} x + B_u \frac{\partial u}{\partial \alpha_i} + \frac{\partial B_u}{\partial \alpha_i} u \tag{7}$$

The solution of this problem is not finite dimensional because of the presence of the $\partial u/\partial \alpha_i$ term. However, several methods[6] exist for approximating $\partial u/\partial \alpha_i$, with the simplest being to assume that $\partial u/\partial \alpha_i$ is small and neglect its contribution.

A second difficulty is the large order of the sensitivity model, which has n states for each of the n_α uncertain parameters. To reduce the control problem to the same order as the LQG problem, the sensitivity states are eliminated through model reduction. Their static effect is maintained, but their dynamic effect is neglected.

With these simplifications, the sensitivity states are a linear combination of the original states of the system and the control. If A^{-1} exists,

$$\frac{\partial x}{\partial \alpha_i} = -A^{-1}\left(\frac{\partial A}{\partial \alpha_i}x + \frac{\partial B_u}{\partial \alpha_i}u\right) \tag{8}$$

Substituting Eq. (8) into Eq. (6) yields a standard LQR problem with modified weighting matrices (R'_{xx}, R'_{xu}, R'_{uu}) of the form

$$R'_{xx} = R_{xx} + \sum_{i=1}^{n_\alpha} \frac{\partial A^T}{\partial \alpha_i} A^{-T} R_{\alpha\alpha_i} A^{-1} \frac{\partial A}{\partial \alpha_i} \tag{9}$$

State estimation is accomplished by applying the dual of the SWLQR, which is simply a Kalman filter with modified noise intensity matrices (V'_{xx}, V'_{xy}, V'_{yy}) of the form

$$V'_{xx} = V_{xx} + \sum_{i=1}^{n_\alpha} \frac{\partial A}{\partial \alpha_i} A^{-1} V_{\alpha\alpha_i} A^{-T} \frac{\partial A^T}{\partial \alpha_i} \tag{10}$$

The additional noise is interpreted as a disturbance entering through the uncertainty. Equations (4) and (5) determine V_{xx}, V_{xy}, V_{yy}, R_{xx}, R_{xu}, and R_{uu}, with $R_{\alpha\alpha_i} = \beta_i R_{xx}$ and $V_{\alpha\alpha_i} = \beta_i V_{xx}$. Thus β_i is the parameter that controls the amount of robustness. The SWLQG controller is obtained by combining this sensitivity-weighted Kalman filter with the SWLQR.

III. MACE Experiments

The MACE test article (Fig. 1) consists of a flexible bus with two payloads, a reaction wheel assembly, and actuators and sensors. Each payload is mounted to the structure by a two-axis gimbal that provides pointing capability. The hardware is suspended using three pneumatic/electric low-frequency suspension devices. The control is implemented using a real-time computer operating at a 500-Hz sampling rate.

Control is designed for a single-input/single-output system with the objective to minimize the rms angular displacement of the primary gimbal z_1 about the X axis with a white-noise input to the X axis of the secondary gimbal w_1. The control input is the primary gimbal X-axis motor u, and the sensor output is the primary gimbal X-axis rate gyro y with sensor noise w_2. The design model is derived from a finite element model (FEM) developed by Glaese.[7] Table 1 lists the frequencies of the important modes of the system, along with the errors in the frequencies when compared to measured data. These errors represent the uncertainty to which the control systems must be robust.

A. Control Synthesis Procedure

Controllers were designed using each of the four control techniques for eight different bandwidths of control. Control bandwidth was altered by varying a weight (ρ) on the control, which is a second performance variable, z_2. Note that $\rho = 0$ is the performance of interest, as long as the controls do not saturate. However, this control problem is singular, and so, ρ must be nonzero.

For each of the robust control techniques, seven modes from Table 1, all except those at 1.39 and 54.16 Hz, were considered uncertain. The relevant robustness weightings in each of the techniques (β_i for SWLQG, δ_i for ME, and the magnitude of frequency shifts in MM) were varied to maximize the performance predicted on the basis of open-loop measured data at each value of ρ.

Each technique was pushed to the maximum bandwidth at which it stabilized the system. Instability for all robust controllers was caused by small gain errors at high frequency accompanied by low gain margin caused by phase lag in the system.

B. Performance Comparison

Eighteen of these controllers were experimentally implemented, with results shown in Figs. 2 and 3. Figure 2 shows the system frequency response in open loop and in closed loop with the best compensator from each technique. It is clear that the MM technique produced the best rms performance. The best ME and SWLQG compensators achieve similar rms performance, whereas LQG was wholly inadequate. Of the LQG controllers, the five with highest bandwidths destabilized the system. Even the best LQG controller exhibits trouble with the mode at 6.8 Hz. What this comparison shows is that for equivalent robustness, i.e., sufficiently robust to the given modeling errors, the performance achieved by these control techniques varies significantly, with MM providing the best performance.

Next, Fig. 3 shows the experimentally measured performance for each controller plotted as a function of the control authority ($1/\rho$). Instability is indicated by performance rising off the chart. The performance predicted by the model for the LQG controllers is also shown. Figure 3 illustrates several important features of the performance/robustness tradeoff. The first is that compared to performance predictions for the model, some performance is sacrificed

Table 1 FEM modal frequencies and errors from data comparison

Description	FEM frequency, Hz	Model error, %
X rotation	1.39	0.0
1st Y bending	3.35	−0.9
1st Violin	6.84	−5.1
2nd Y bending	9.42	1.3
2nd Violin	13.74	−5.2
3rd Y bending	18.73	9.8
4th Y bending	23.32	7.5
5th Y bending	50.42	3.8
6th Y bending	54.16	0.3

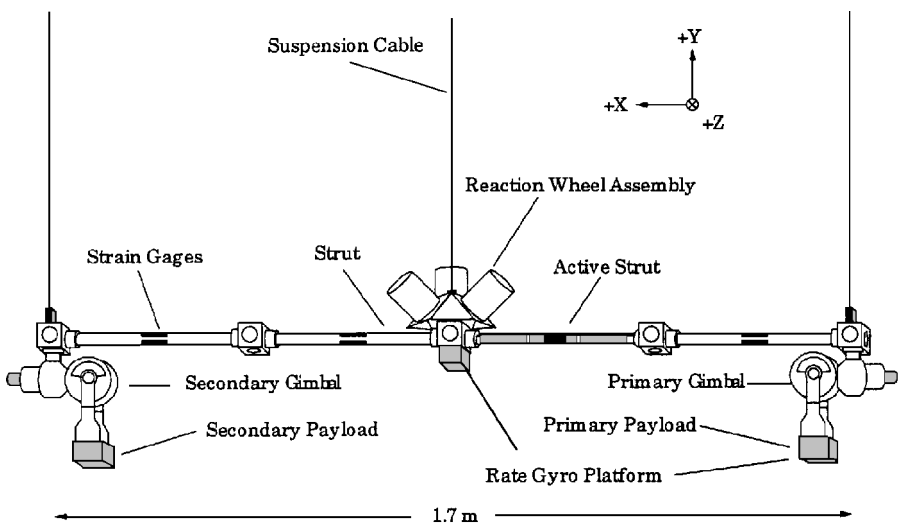

Fig. 1 MACE test article suspended in 1 *g*.

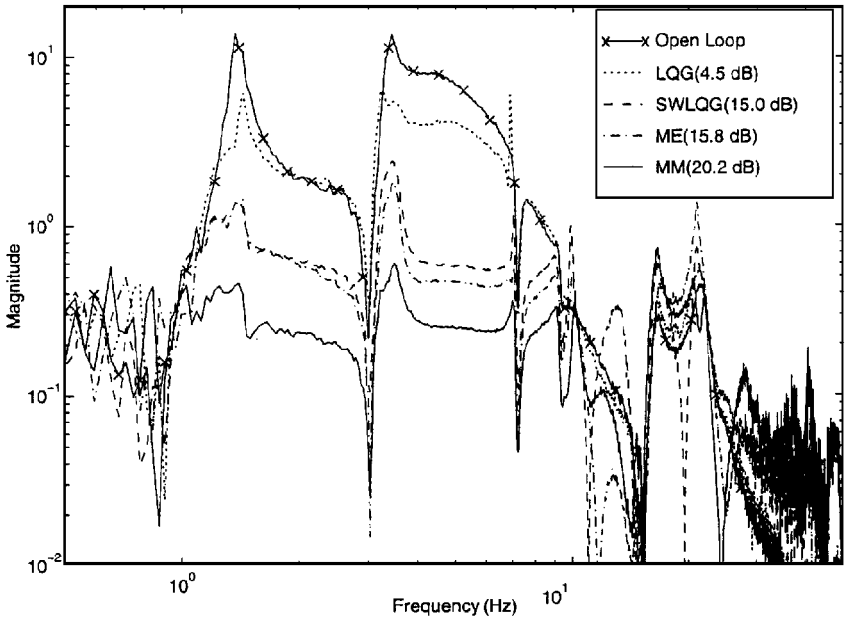

Fig. 2 Performance frequency response for open loop and best controller for each $\mathcal{H}_2$ control technique.

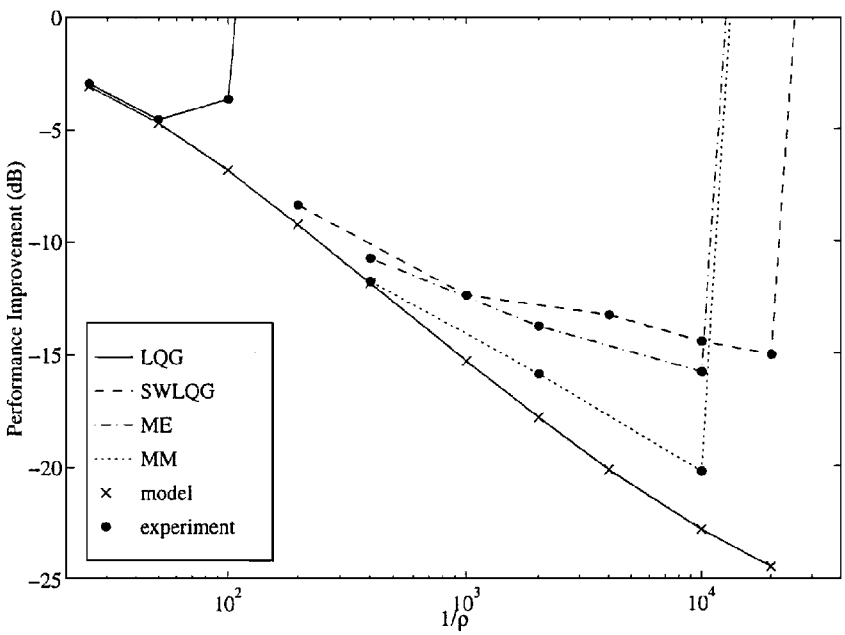

Fig. 3 Experimentally measured performance as a function of control authority, with predicted LQG performance.

by the robust techniques in order to improve robustness. This can be seen by the gap between the performance of the robust controllers and that predicted by the model for LQG. Note that the performance gap is much smaller for MM than either ME or SWLQG. However, because of model errors, the higher-authority $\mathcal{H}_2$ optimal LQG controllers are not sufficiently robust. By contrast, the robust controllers are sufficiently robust to the parameter errors to remain stable and achieve good performance (though less than LQG predicts with the model). Thus robustness to frequency uncertainty has allowed these controllers to achieve better performance than LQG by permitting higher bandwidth control. Of these, MM achieved the best, more than 10 times (20 dB) better than open loop.

IV. Conclusions

The experimental results for this design problem show that for equivalently robust controllers, MM control provides the highest performance (> 20 dB) of all of the control techniques. ME and SWLQG provided similar performance, with ME marginally better than SWLQG. $\mathcal{H}_2$ optimal LQG was inadequate, providing only 4.8-dB rms performance improvement. These results illustrate the paradox that, for robust control techniques, although performance on the nominal design model is sacrificed compared to $\mathcal{H}_2$ optimal control in order to improve robustness, performance on the actual system is gained because higher authority control can be implemented.

References

[1] Sesak, J. R., "Sensitivity Constrained Linear Optimal Control Analysis and Synthesis," Ph.D. Thesis, Dept. of Electrical and Computer Engineering, Univ. of Wisconsin–Madison, WI, 1974.

[2] Hyland, D. C., "Maximum Entropy Stochastic Approach to Controller Design for Uncertain Structural Systems," *Proceedings of the American Control Conference* (Arlington, VA), American Automatic Control Council, New York, 1982, pp. 680–688.

[3] Collins, E. G., Jr., King, J. A., and Bernstein, D. S., "Application of Maximum Entropy/Optimal Projection Design Synthesis to a Benchmark Problem," *Journal of Guidance, Control, and Dynamics*, Vol. 15, No. 5, 1992, pp. 1094–1102.

[4] Ashkenazi, A., and Bryson, Jr., A. E., "Control Logic for Parameter Insensitivity and Disturbance Attenuation," *Journal of Guidance, Control, and Dynamics*, Vol. 5, No. 4, 1982, pp. 383–388.

[5] Kwakernaak, H., and Sivan, R., *Linear Optimal Control Systems*, Wiley-Interscience, New York, 1972, Chap. 5.

[6] Weinmann, A., *Uncertain Models and Robust Control*, Springer–Verlag, New York, 1991, Chap. 10.

[7]Glaese, R. M., and Miller, D. W., "On-Orbit Modelling of the Middeck Active Control Experiment from 1-*g* Analysis and Experimentation," *Proceedings of the International Modal Analysis Conference* (Honolulu, HI), Society for Experimental Mechanics, Bethel, CT, 1994, pp. 1107–1113.

Integral Relations for Disturbance Isolation

Boris J. Lurie*
Jet Propulsion Laboratory,
California Institute of Technology,
Pasadena, California 91109-8099

Introduction

PASSIVE and active dynamic systems of high order are employed for the purpose of disturbance isolation. Such systems' theory and design methods could benefit from using the design theory of active electrical networks.[1] The feasibility and the available performance of such systems can be evaluated using Bode integrals. This enables the system engineer to resolve the design tradeoffs without actually designing the system and the subsystems. A Bode integral is applied to estimate the performance of a disturbance isolation system.

Consider the system in Fig. 1a of two bodies connected with an active strut,[2] which is a linear motor. A force disturbance source F_1 is applied to the body M_1 (capital letters designate Laplace transforms). The force F_3 is applied via the massless active strut to the body M_3. To increase the disturbance isolation, the force division ratio $K_F = F_3/F_1$ should be made small. The strut mobility (in some literature called mechanical impedance) Z_2 is the ratio of the difference in the velocities at the ends of the strut to the force (because we neglect the strut's mass, the force is same at the both ends of the strut). Feedback is employed in the active strut to increase $|Z_2|$ in order to reduce $|K_F|$.

For the purpose of analysis we use the following electromechanical analogy: power to power, voltage to velocity, current to force, capacitance to mass, and inductance to the inverse of the stiffness coefficient. The electrical equivalent circuit for the system is shown in Fig. 1b. The current division ratio I_3/I_1 is equivalent to K_F. The electrical impedance Z_2 is the equivalent of the strut mobility.

The current division ratio, i.e., the force division ratio, is

$$K_F = \frac{1/(sM_1)}{1/(sM_1) + Z_2 + 1/(sM_3)}$$

or

$$K_F = \frac{1}{1 + sM_1Z_2 + M_1/M_3} \tag{1}$$

At higher frequencies, the strut equivalent electrical impedance in Fig. 1b degenerates into the impedance of the series inductance included in Z_2, the inductance being equivalent to the inverse of the stiffness coefficient k of the strut at higher frequencies. Therefore, the force division ratio at higher frequencies turns into

$$K_F|_{\omega\to\infty} = k/s^2M_1 \tag{2}$$

Because this value reduces as a square of the frequency, Bode integral of the real part of a function[1,3] applies. From this integral,

$$\int_0^\infty \log|K_F + 1|\,\mathrm{d}\omega = 0 \tag{3}$$

Received Sept. 23, 1996; revision received Dec. 10, 1996; accepted for publication Dec. 23, 1996. Copyright © 1997 by the American Institute of Aeronautics and Astronautics, Inc. The U.S. Government has a royalty-free license to exercise all rights under the copyright claimed herein for Governmental purposes. All other rights are reserved by the copyright owner.

*Member, Technical Staff, Guidance and Control Analysis Group, Automation and Control Section. Member AIAA.

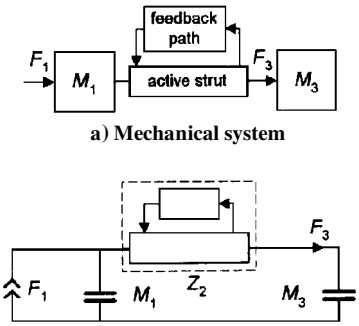

Fig. 1 Two-body system.

This relation remains valid with and without feedback in the active strut and allows one to estimate the effect of feedback on the disturbance isolation at higher frequencies, but only as long as the Fig. 1 model correctly reflects the physical strut and the bodies. The model must be accurate enough over the frequency range where $\log|K_F + 1|$ is substantial. The model might become inaccurate at higher frequencies within this range because the mass of the strut cannot be neglected at high frequencies and the bodies cannot be considered rigid. Integral relations can be developed for such systems as well[1]; however, the increased complexity of the integrand makes it more difficult to use the relations for fast performance estimation while comparing different design versions.

Another equation, which will give a better estimation of the available performance at lower frequencies, can be found as follows. From Eq. (1),

$$\frac{1}{K_F(1 + M_1/M_3)} = 1 + \frac{sM_1Z_2}{1 + M_1/M_3} \tag{4}$$

Consider the practical case of the feedback in the active strut to be finite at dc. At lower frequencies, the active strut degenerates into some spring. Therefore, at lower frequencies the fraction in the right-hand side of Eq. (4) increases with frequency as ω^2. With the frequency scale inverted, the fraction decreases at high frequencies as ω^{-2}. Then the Bode integral of the real part of a function applies, and from the integral, the integral of the logarithm of the expression in the right side of Eq. (4) equals 0. Therefore,

$$\int_0^\infty \left[-\log|K_F| - \log\frac{1 + M_1}{M_3}\right]\mathrm{d}\omega^{-1} = 0$$

or

$$\int_0^\infty \log|K_F|\,\mathrm{d}\omega^{-1} = -\int_0^\infty \log\frac{1 + M_1}{M_3}\,\mathrm{d}\omega^{-1} \tag{5}$$

The feedback in the active strut does not affect the right-hand side of the equation. Therefore, when comparing the cases with different values of feedback in the active strut loops, the right-hand part of Eq. (5) can be neglected. Hence, the integral of the difference in the vibration transmission between any two cases with different feedback in the active strut is zero:

$$\int_0^\infty \Delta\log|K_F|\,\mathrm{d}\omega^{-1} = 0 \tag{6}$$

Equation (6) is important because it places a simple fundamental restriction on what can be achieved by disturbance isolation design. Introduction of feedback in the active strut reduces the force division ratio at some frequencies, but at some other frequencies (in fact, at lower frequencies) this ratio increases, and the difference in the areas of the output force reduction and the force increase, with inverse frequency scale, is zero.

In experiments with a large-scale model of an interstellar interferometer, a vibration source (representing a reaction wheel) was placed on a platform (body 1) suspended on six orthogonal active struts. Vibration propagation to the base on which sensitive optics was installed (body 2) was reduced by the bandpass feedback in the active struts by 30 dB at 20 Hz, the value gradually decreasing with